Electronic structure of a two-dimensional alloy: Sn–Pb–Si on Si(111)



2004 J. Phys.: Condens. Matter 16 3507

(http://iopscience.iop.org/0953-8984/16/21/001)

INSTITUTE OF PHYSICS PUBLISHING JOURNAL OF PHYSICS: CONDENSED MATTER

J. Phys.: Condens. Matter **16** (2004) 3507–3516 PII: S0953-8984(04)74710-4

# Electronic structure of a two-dimensional alloy: Sn–Pb–Si on Si(111)

**C Di Teodoro[1], B Ressel[2,3,5], K C Prince[2,4], V Cháb[3], S Santucci[1], S Faccani[1], G Profeta[1] and L Ottaviano[1,6]**

[1] Istituto Nazionale di Fisica della Materia (INFM) and Dipartimento di Fisica, Università degli Studi dell'Aquila, I-67010 Coppito (L'Aquila), Italy
[2] Sincrotrone Trieste, Strada Statale 14, Km 163.5, 34012 Basovizza-Trieste, Italy
[3] Institute of Physics of the Academy of Science of the Czech Republic, Cukrovarnická 10, 16253 Prague 6, Czech Republic
[4] TASC, INFM, in Area di Ricerca, Strada Statale 14, Km 163.5, 34012 Basovizza-Trieste, Italy

E-mail: luca.ottaviano@aquila.infn.it

Received 14 January 2004
Published 14 May 2004
Online at stacks.iop.org/JPhysCM/16/3507
DOI: 10.1088/0953-8984/16/21/001

**Abstract**

Scanning tunnelling microscopy and core level photoemission spectroscopy experiments demonstrate that an ordered surface reconstruction of Pb, Sn and Si adatoms (1/3 monolayer overall coverage) can be formed with $\sqrt{3}\times\sqrt{3}$R30° symmetry on the Si(111) substrate. Pb, Sn and Si atomically intermix, occupying $T_4$ sites as in the case of the well known pure 1/3 ML Sn or Pb $\sqrt{3}\times\sqrt{3}$R30° reconstructions. The electronic structure of this surface, investigated with scanning tunnelling spectroscopy and valence band photoemission, shows a semiconducting behaviour (0.4 eV bandgap), and two surface bands centred at ±0.7 eV with respect to the Fermi level. These features are significantly different from those of the electronic structure of the binary Pb–Si/Si(111) and Sn–Si/Si(111) 2D alloys. This occurrence demonstrates that tailoring the electronic structure of a surface alloy is viable just by mixing adatoms with the same valence and different sizes.

## 1. Introduction

Tailoring the physical properties of bulk alloys by varying the composition of metal species and their concentration has been the main goal of metallurgy since its early days. Applying these concepts to reduced dimensionality systems is rather intriguing. For example, a recent paper which has attracted considerable attention in the field of low dimensional physics concluded

[5] Present address: TASC, INFM, in Area di Ricerca, Strada Statale 14, Km 163.5, 34012 Basovizza-Trieste, Italy.
[6] Author to whom any correspondence should be addressed.

  

with the suggestion of engineering the Fermi surface of a two-dimensional (2D) alloy by deposition of different metal adatom species on the same substrate [1]. The first step toward this goal is to demonstrate that the fabrication of such surface alloys is viable and to investigate their electronic structure. 2D alloyed surfaces can be of the type $A_{(1-x)}B_x$ as the topmost layer on a bulk alloy substrate $A_{(1-y)}B_y$ [2], or of the type $A_{(1-x)}B_x$/B, as a result of surface intermixing of A type adatoms with B type substrate adatoms [3–5], or two-dimensional alloys $A_{(1-x)}B_x$/C with A and B type adatoms on a substrate C. In this case there are often C atoms at the surface, which then becomes a ternary system. There are rather few examples of the latter type with little insight into the structural and electronic properties of the two-dimensional alloy [6–8]. Among surface alloys of the second type, the 1/3 ML $Sn_{(1-x)}Si_x$/Si(111) [3] and the $Pb_{(1-x)}Si_x$/Si(111) [4] systems ($0 < x < 0.5$) are truly two-dimensional binary alloys, due to the bulk immiscibility of Pb and Sn with the Si substrate [9]. These two solid solutions of isovalent group IV adatoms, known in the limiting case of $x = 0.5$ as mosaic or $\gamma$ phases, are very alike. Both show the same $\sqrt{3} \times \sqrt{3}$R30° reconstruction (hereafter $\sqrt{3}$ for brevity) with the adatoms occupying the $T_4$ adsorption sites, and similar short range order features [3]. The typical temperatures required to obtain the 1/6 ML coverage of Sn and Pb are in contrast very different: 850 and 350 °C for Sn and Pb respectively. Moreover, although they do not form intermetallic phases and their mutual solid solubility is limited, Pb and Sn are highly miscible in the liquid state [10]. The liquid is a state which is not highly constrained, suggesting that the miscibility may also be high in another situation which is not constrained, namely a two-dimensional system. All these properties lead one to speculate that for the $\gamma$ phases of Sn and Pb on Si(111) a purely two-dimensional mixture of Pb and Sn adatoms sitting in $T_4$ sites on the Si(111) substrate might be stable. In this case, one could investigate the structural and electronic effects of alloying in a purely two-dimensional system of atomic species with the same valence, differing mainly in the atomic size. In this paper we report the preparation and the experimental investigation of the structural and electronic properties of a two-dimensional Pb–Sn–Si ternary alloy on a Si(111) substrate, using the $\gamma$-Sn/Si(111) mosaic surface as a template.

## 2. Experimental details

The low energy electron diffraction–scanning tunnelling microscopy (LEED–STM) experiments were performed with ultra-high vacuum (UHV) systems described elsewhere [11, 12]. The photoemission experiments were performed in a UHV chamber of base pressure $2.6 \times 10^{-10}$ mbar (connected in UHV by means of transfer tubes with the STM–LEED equipment of [12]) equipped with a monochromatized Al K$\alpha$ source ($h\nu = 1486.6$ eV) for x-ray photoelectron spectroscopy (XPS), a helium discharge lamp for ultraviolet photoemission spectroscopy (UPS) and a hemispherical analyser (model 10-360 from Physical Electronics). The angle between the photon beam and the analyser axis was 90° and 57° for the x-ray and the UV source respectively. The x-ray source was operated at 14 kV, with an emission current of 25 mA. The ultra-violet (UV) lamp was operated at a He pressure of $6.5 \times 10^{-8}$ mbar. The analyser settings yielded an energy resolution of 0.5 eV half width at half maximum (HWHM) during acquisition of XPS survey spectra (600 eV energy span) performed to detect surface contaminants, and of 0.15 eV (0.20 eV) HWHM during acquisition of detailed UPS (XPS) spectra (as measured at the Fermi level of the Mo clips of the sample holder). The analyser acceptance angle was always set to ±7°. For HeI radiation this gives a $k_\parallel$ acceptance of ±0.25 Å$^{-1}$. In both XPS and UPS, data are taken at 30° from normal emission along the **ΓM** direction. In $k_\parallel$ space this approximately corresponds to the centre of the second Brillouin zone of $\sqrt{3}$

reconstructed surfaces on Si(111). Under these conditions the HeI spectra are partially angle integrating around the $\Gamma$ point within a radius of $k_{\parallel} = 0.25$ Å$^{-1}$ ($\|\Gamma\mathrm{M}\| = 0.55$ Å$^{-1}$). In both the experimental set-ups of [11] and [12], Pb and Sn were deposited by using two electron beam evaporators (EFM3 Focus, Omicron Ltd) equipped with flux monitors for determination of the evaporation rates. The $\gamma$-Sn/Si(111) template surface was prepared by the procedure described in [3] and a clear LEED pattern with $\sqrt{3}$ symmetry was detected. Then approximately 1.5 ML Pb was deposited at room temperature. LEED of this Pb/$\gamma$-Sn/Si(111) interface showed a uniform background with no diffraction spots. After annealing the surface at 350 °C (as in the procedure to prepare the 1/6 ML $\gamma$-Pb/Si(111) surface [4]) again one obtains a clear and sharp LEED pattern with $\sqrt{3}$ symmetry. During the STM experiments, the Pb source was mounted pointing at the STM sample stage. Thus we could scan on the mosaic Sn/Si(111) surface first, then retract the tip, evaporate Pb, anneal the surface and point the tip at the same location of the sample (within the 1 $\mu$m lateral accuracy of the coarse approach stage). An identical surface preparation procedure was followed during photoemission experiments. LEED was used at each step to check the quality of the surface reconstruction after flashing the Si substrate, and annealing after Sn and after Pb deposition. XPS spectra are presented as taken. UPS spectra are presented after subtraction of a third order polynomial background, and the energy was calibrated to the Fermi level of the Mo clips of the sample holder after each measurement. The samples were first characterized with XPS in order to check for the correct Sn/Pb ratio at the surface, then the UPS spectra were acquired without changing the sample–analyser relative position. With this procedure, the UPS spectra can be assigned to the same sample area (0.8 mm diameter) as viewed by the analyser during acquisition of the XPS spectra. This is a crucial experimental point, as the Pb and Sn concentrations along the sample surface can vary significantly (from 1/9 ML up to 1/3 ML), on a few millimetre length scale. This is due to local variations of the Pb and Sn desorption rate from the surface owing to thermal gradients typically observed along the sample surface during the annealing. The scanning tunnelling spectroscopy (STS) data are presented in the form of normalized conductance curves calculated from $I$–$V$ curves obtained by averaging 1600 single $I$–$V$ curves. Images with atomic resolution were routinely obtained during the acquisition of the $I$–$V$ spectra, indicating the stability of the tip–sample vacuum gap during the time of the interrupted feedback loop for $I$–$V$ acquisition. Different sets of data have been taken by varying the set-point voltage, with the set-point current fixed (i.e. at different tip–sample distances). The scale of STM vertical displacement was calibrated on a reference Si(111)7 × 7 surface.

## 3. Results and discussion

Figure 1(a) is a filled state STM image of the $\gamma$-Sn/Si(111) surface, with 50% Sn adatoms [3, 13, 14]. Sn (Si) adatoms are typically bright (dark) in filled state STM images above 1.8 V negative sample bias. The apparent height ripple between the Si adatoms and the Sn first (third) neighbours in filled state images is $1.5 \pm 0.1$ Å ($1.1 \pm 0.1$ Å). The same values correspond to 0.6 Å (0.5 Å) in empty state images. The height corrugation value measured with STM is significantly influenced by electronic effects [12] and is believed to approach the real structural corrugation in empty state images. First principles calculations show that the structural height difference between Sn and Si adatoms in a $T_4$ site on the Si(111) substrate is 0.74 Å [13, 14]. This structural corrugation is mainly due to the different atomic sizes of Sn and Si. After 1.5 ML Pb nominal deposition (and annealing at 350 °C) the same surface, at the same tunnelling set-point, shows the appearance of figure 1(b). Most of the dark sites have disappeared, leaving a remaining concentration of 21% of dark adatoms: these atoms are

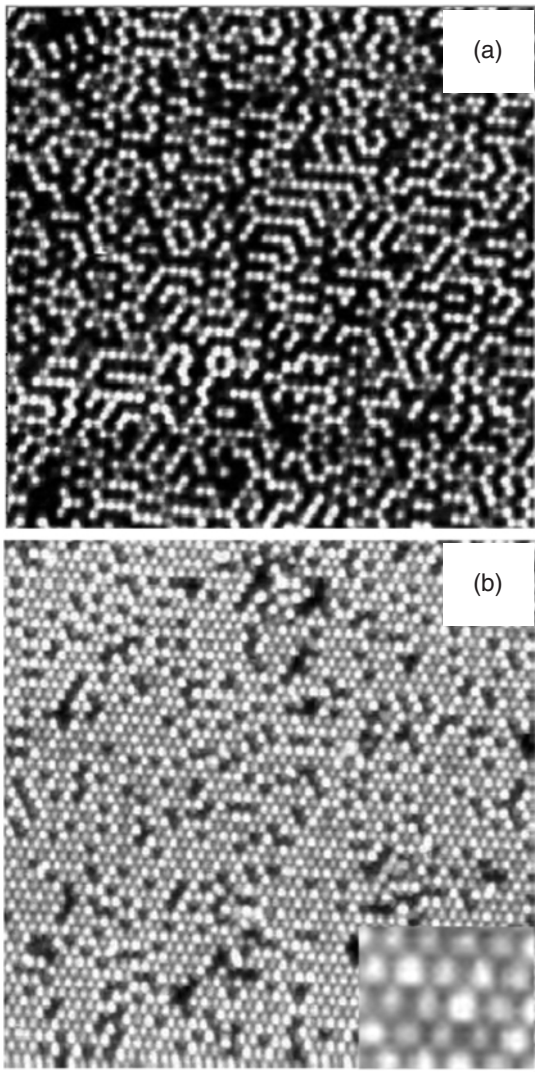


**Figure 1.** STM filled state images ($32 \times 32$ nm$^2$) of two-dimensional alloyed $\sqrt{3} \times \sqrt{3}$R30° surfaces on Si(111). (a) $\gamma$ phase, $Si_{0.5}Sn_{0.5}$/Si(111) ($-1.9$ V, 0.3 nA); Sn (Si) adatoms are bright (dark). (b) 1/3 ML ($Si_{0.2}Sn_{0.5}Pb_{0.3}$)/Si(111) ($-2.1$ V, 0.3 nA); Si adatoms occupy the dark sites. The lower right inset is a magnified scan that illustrates isolated higher adatoms.

assigned to Si adatoms. They follow the same bias dependent vertical corrugation measured for the Si adatoms on the 1/3 ML $Sn_{(1-x)}Si_x$/Si(111) surface as in [3]. Figure 2 shows various filled and empty state images of the surface of figure 1(b). In this figure each pair of panels is taken on the same area, but each voltage is on a different area. It is evident from STM that Pb adatoms have partly substituted the Si adatoms on the surface, forming a Pb–Sn–Si ternary solid solution. Hereafter for brevity we refer to it as the Pb–Sn surface. Preliminary first principles calculations indicate that the 1/3 ML $Pb_xSn_{(1-x)}$/Si(111) ($0.33 < x < 0.5$) system is stable against phase separation [15], which is also to be expected for reasons outlined above. It is difficult to decide from the STM images alone which atoms are Pb and which Sn. A careful

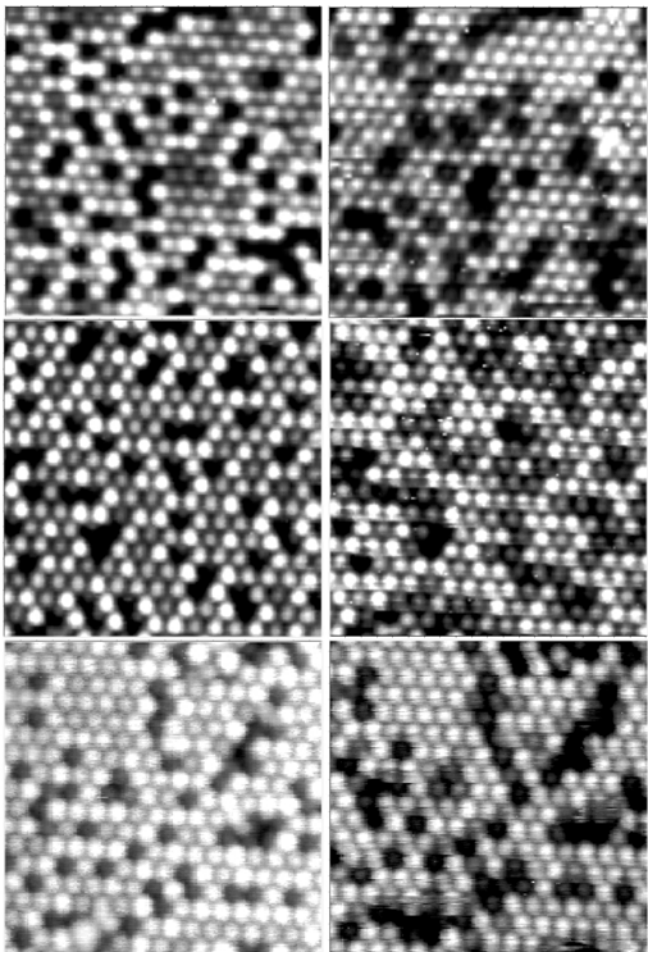

**Figure 2.** Voltage dependent STM images ($100 \times 100$ Å$^2$) of the (Sn–Pb)/Si(111)$\sqrt{3} \times \sqrt{3}$R30° surface. Left-hand panels, filled state images; right-hand panels, empty state images. Voltage from top to bottom: 2.1, 1.4 and 0.6 V. Set-point current: 0.2 nA.

visual inspection of the filled state STM images of the Pb–Sn alloyed surface indicates the presence of isolated adatoms with increased apparent height; e.g. see the lower right inset of figure 1(b). These adatoms are quite distant (at least second nearest neighbours) from Si adatoms. So their apparent height is not influenced by the Si defect induced perturbation, that is limited to their first neighbours [12]. These isolated brighter adatoms are 0.4 Å (0.2 Å) higher than their neighbours in filled state (empty state images). In this case, it can be speculated that they are Pb adatoms, since 0.35 Å is the difference between the Pb and Sn atomic radii. The mechanism of Pb–Si partial substitution that takes place on the $\gamma$-Sn/Si(111) template is likely to be assisted by step edges acting as Si reservoirs.

The experimental results of figure 3 provide quantitative information about the chemical identity of the species adsorbed on the surface of figure 1(b). This figure shows the XPS results obtained on a sample surface prepared with an identical procedure to that of figure 1(b) and showing a sharp $\sqrt{3}$ LEED pattern. Panel (a) shows the presence of Sn and Pb on the surface. Carbon and oxygen are not detected within the sensitivity limit of this technique

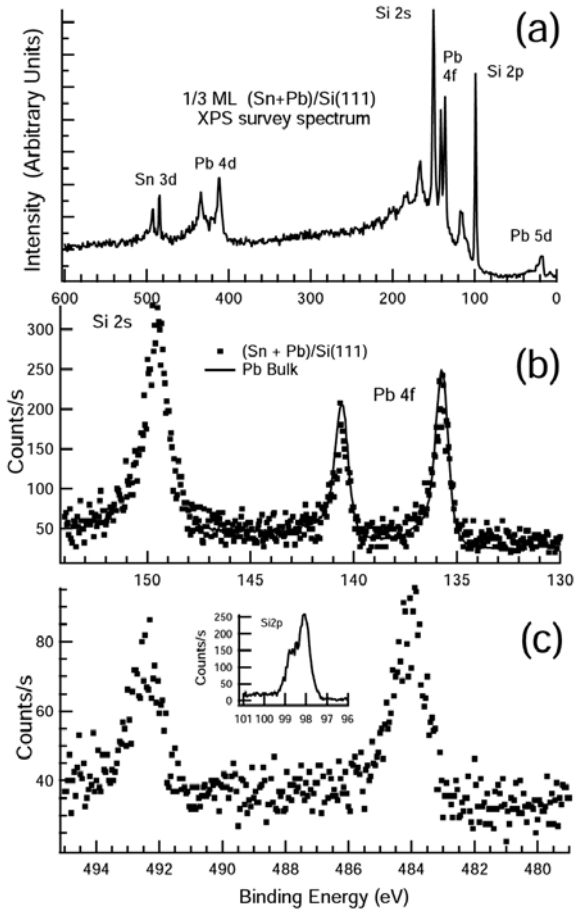


**Figure 3.** XPS (Al K$\alpha$ source) core level spectra of the (Pb–Sn)/Si(111)$\sqrt{3} \times \sqrt{3}$R30° surface. (a) Survey spectrum showing the Sn, Pb and Si core level peaks. (b), (c) High resolution (0.2 eV HWHM) Pb 4f and Sn 3d spectra. Solid curve in panel (b): Pb 4f core level of bulk Pb. Inset in panel (c): Si 2p core level spectrum.

(1%). Panels (b) and (c) are the Pb 4f and Sn 3d core level spectra taken with higher energy resolution. The Pb $4f_{7/2}$/Sn $3d_{5/2}$ peak area ratio provides a direct estimate of the relative Pb/Sn concentration. Once the Pb and Sn sensitivity factors are taken into account [16], this ratio is $1.0 \pm 0.2$ for the XPS data in panels (b) and (c). This chemical analysis corroborates the experimental result that a $\sqrt{3}$ symmetry over-layer of a Pb–Sn alloy can be formed on the Si(111) substrate. Evidently, as in the 2D $Sn_{(1-x)}Si_x$/Si(111) solid solution [3], the ratio between the adatoms of different chemical species does not influence the surface symmetry. The adatom adsorption sites remain $T_4$, as clearly shown by STM.

The electronic density of states of the Pb–Sn alloy has been investigated with UPS and STS. Figures 4 and 5 summarize the experimental findings. Figure 4 reports $I$–$V$ spectra taken on the (Pb + Sn)/Si(111) surface (a), and on the two mosaic surfaces $\gamma$-Sn/Si(111) (b) and $\gamma$-Pb/Si(111) (c). Three data sets (dot–dashed, solid and dashed curves) have been taken at different (1.4, 1.6 and 1.8 V) set-point voltages (same set-point current 0.3 nA) in order to highlight, if present, variations of the peak intensities owing to dispersion in $k$ space of

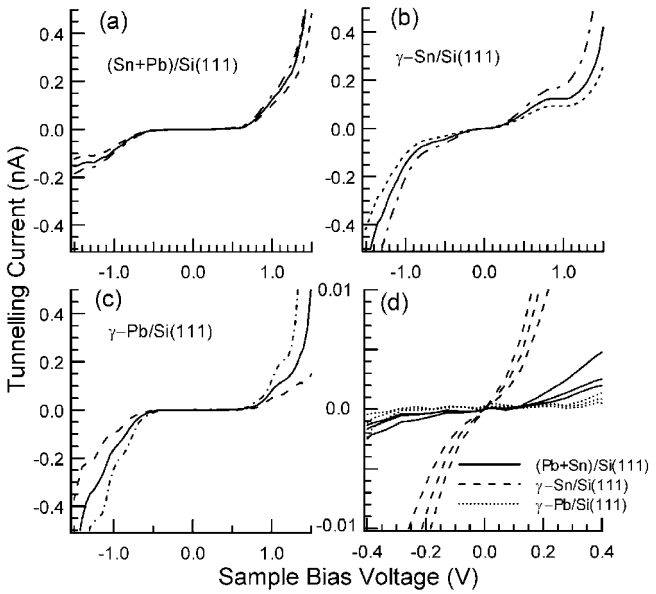


**Figure 4.** STS $I$–$V$ curves for (a) the (Sn + Pb)/Si(111) phase (taken on the sample area of the $\sqrt{3} \times \sqrt{3}$R30° (Pb–Sn)/Si(111) of figure 1(b)), (b) the $\gamma$-Sn/Si(111) phase and (c) the $\gamma$-Pb/Si(111) phase. In each panel (from (a) to (c)) three curves are reported taken at fixed set-point current ($I = 0.3$ nA) and with set-point voltage of 1.4 V (dot–dashed curve), 1.6 V (solid curve) and 1.8 V (dashed curve). Panel (d) reports the central part, around zero sample bias voltage, of the curves shown in (a), (b) and (c).

the spectral features [17]. Panel (d) shows, magnified, the central part of the three sets of curves (a), (b) and (c). The $I$–$V$ curves for the different phases at different set-point voltages all show very good reproducibility. Moreover, each data set has its own peculiar features. This indicates that each surface has its own electronic structure and that the densities of states (DOSs) of the three systems are different one from another. The graphs shown in panel (d) are of importance for they give information on the metallic or semiconducting nature of the surfaces under investigation. The (Pb + Sn)/Si(111) spectra lie in between those of the other two parent phases. The surface bandgap (the voltage region where the tunnelling current is negligible and below the instrumental current sensitivity limit of 1 pA) of this ternary alloy can be estimated as of the order of 0.4 eV $\pm$ 0.1, whereas $\gamma$-Pb/Si(111) has a bandgap value of 0.7 $\pm$ 0.1 eV. The bandgap is closed for $\gamma$-Sn/Si(111). Other features in the DOS of the three phases are better evidenced in the normalized conductance spectra presented in figure 5. In this figure, the curves (calculated from the $I$–$V$ spectra of figure 4) taken at different set-point voltages show excellent reproducibility. They almost superimpose. The spectra of the (Pb + Sn) phase (top panel) show a 0.7 eV wide band at 0.7 eV below the Fermi level ($E_{\mathrm{F}}$), or 0.0 V bias voltage for STM. In the empty states (positive sample bias) there is a narrow, 0.4 eV wide, peak at +0.7 eV. In this energy range there are two minima in the local density of states (DOS) of the surface, at $-1.3$ eV below $E_{\mathrm{F}}$ and 1.2 eV above $E_{\mathrm{F}}$. In the same panel is also reported for direct comparison the UPS spectrum (open circles) of the same Pb–Sn sample of figure 3(a) taken at the same spot where the XPS data were acquired. The UPS data are reported at the negative sample bias side (corresponding to filled surface states) after intensity rescaling in order to match the corresponding STS peak intensity values. There is

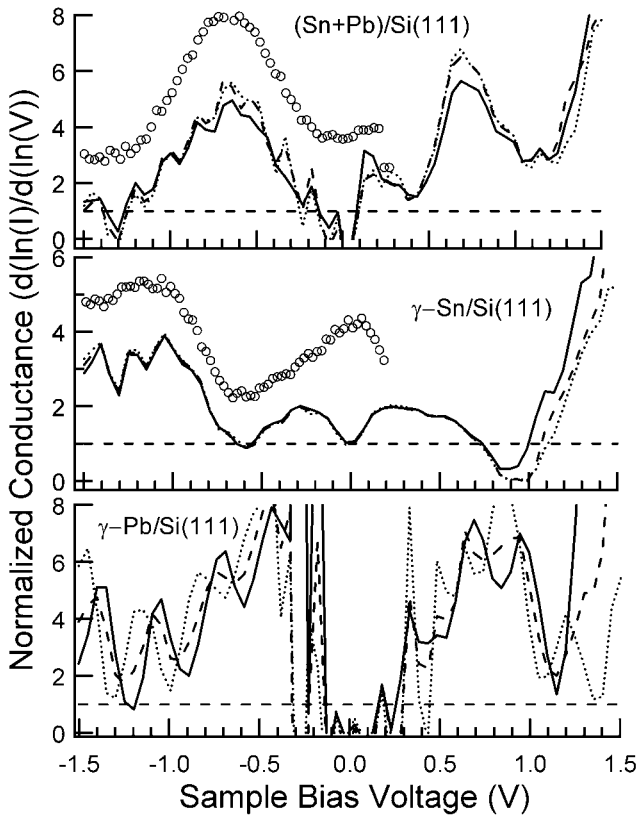


**Figure 5.** Top panel: normalized conductance curves from the $I$–$V$ spectra of figure 4(a). Curves are plotted with corresponding line-styles. Open circles: UPS spectrum of an identically prepared (Pb–Sn)/Si(111) system after an arbitrary intensity renormalization (the curve is vertically displaced for better clarity). Horizontal line: normalized conductance = 1. Middle and bottom panels: the same as in the top panel but for the $\gamma$-Sn/Si(111) and $\gamma$-Pb/Si(111) phases respectively.

very good agreement between the UPS and the STS data taken on the Pb–Sn system[7]. In the middle panel of figure 5 we compare the STS spectrum of the $\gamma$-Sn/Si(111) surface before Pb deposition. Again superimposed on the filled state region of the STS data are the UPS data (open circles) of an identically prepared surface. Also in this case there is excellent agreement between the two data sets. We shall discuss elsewhere the electronic properties of this system [18]. Most important for our discussion is the fact that simple visual inspection of figure 5 (top) and (middle) shows that the electronic structure before and after Pb deposition on this surface is changed. Also interesting is the comparison with the electronic structure of

[7] The deviation of the UPS from the STS data close to the Fermi level is a consequence of the rescaling procedure. This follows from the fact that the normalized conductance in STS is not rigorously directly proportional to the DOS of a surface. It is also worth noting that STS is not simply an angle integrating technique, as electronic states with different parallel momentum $k_\parallel$ have a tunnelling probability proportional to the exponential factor

$$\exp\left(-2z\sqrt{2m_e\bar{\phi}/\hbar^2 + k_\parallel^2}\right)$$

(where $z$ is the tip–sample distance, and $\bar{\phi}$ the average tip–sample work-function). Thus STS mostly weights the electronic density of states near the $\Gamma$ point. This further justifies the agreement found between STS and UPS, as our UPS data are angle integrating around the $\Gamma$ point.

$\gamma$-Pb/Si(111). The normalized conductance spectra of this phase are reported in the bottom panel of figure 5(c). The features of these STS spectra are similar to those of our Pb–Sn alloy, but the energy separation between the two bands on either side of the Fermi level (0.0 bias voltage) is 0.2–0.3 eV smaller for the Pb/Si mosaic system. For the sake of completeness it is worth recalling the main features of the electronic structure of the pure metallic $\alpha$-Sn/Si(111) and $\alpha$-Pb/Si(111) phases. They are very similar to one another but still different from those of the Pb–Sn alloy, as evidenced by angle resolved UPS experiments [19, 20]. In particular, both $\alpha$-Sn/Si(111) and $\alpha$-Pb/Si(111) have a low density of states exactly in the energy window 0.4–0.9 eV below $E_F$, where the filled DOS of the Pb–Sn mixture reaches its maximum.

Thus, we have demonstrated that the simple substitution in the Sn–Si alloy of Si adatoms with adatoms of larger size and the same valence (namely Pb) produces a novel surface electronic structure, with maximum density of states at $\pm 0.7$ eV with respect to the Fermi level, and different from those of the closely related $\sqrt{3}$ reconstructions of pure or mixed (metal–semiconductor) group IV adatoms.

Two factors influence the surface electronic structure of these alloys, namely, the surface rippling due to differences in the adatoms' sizes [14, 15], and the surface short range chemical order [3, 15]. First principles calculations performed on group IV binary alloys onto Si(111) describe the former effect [14, 15]. We have demonstrated that, once the relaxed structure of the $\alpha$-Sn/Si(111) surface is considered, then any chemical substitution of Sn with Si, or Pb, or any group IV atom, has a negligible effect on the electronic structure of the host $\alpha$-Sn/Si(111) surface, that remains metallic. This is sound, as all these adatoms have the same valence. Instead, when the structure of the surface alloy is allowed to relax, a surface rippling emerges due to the differences in the adatoms' sizes. This surface rippling is accompanied by a bandgap opening and surface band decoupling [14, 15]. The filled state band is localized on the larger adatoms and the empty state band on the smaller ones. As a rule of thumb, for larger adatom size difference, the surface bandgap is larger and the band decoupling is more effective [14]. On the other hand, in a given binary alloy, the outward relaxation of the larger adatom is also a monotonically increasing function of the number of unlike smaller nearest neighbouring (NN) adatoms [14, 15]. Accordingly, in a real binary alloy, there can be local variations of effective surface band decoupling due to the different types of short range order [15]. This ultimately produces on average a broadening of the surface bands, that is larger for surfaces with a larger degree of chemical disorder.

These arguments help us to understand the features of the electronic structures of the binary alloys, where the two above mentioned effects can be somewhat quantified. For example, the Pb–Si adatoms' size difference is obviously larger than the one between Sn and Si. Moreover, we have quantitatively demonstrated that the number of unlike first neighbours of the larger adatom is higher for $\gamma$-Pb/Si(111) than for $\gamma$-Sn/Si(111) [3]. This latter system is definitely much less short range ordered. Accordingly, the surface band decoupling is by far more effective in the $\gamma$-Pb/Si(111), that is semiconducting, than in $\gamma$-Sn/Si(111), that has zero bandgap width. For our ternary phase, the picture is of course more complicated. It is not simply a binary Sn + Pb phase. Si adatoms are significantly present at the surface. As clearly indicated by STM, Pb and Sn distinction is quite difficult. Accordingly a quantitative determination of the short range order features of this alloy is not viable. Nonetheless, the above mentioned effects of adatoms' size induced surface band decoupling, and band broadening due to chemical disorder, evidently play a role, as indicated by the experimental evidence: this phase shows an intermediate electronic structure between those of the two parent Pb–Si and Sn–Si binary phases.

To summarize, we have experimentally prepared a two-dimensional solid solution of Pb, Sn and Si adatoms on a Si(111) substrate. This surface shows a $\sqrt{3} \times \sqrt{3}$R30° reconstruction

and has its own characteristic electronic structure different from those of other group IV $\sqrt{3}$ induced reconstructions on Si(111).

Finally, it is worth proposing some future experimental developments for electronic structure engineering of 2D systems. Firstly, the mutual concentration of the two adatom species can be varied. Then, the valence of one of the two adatoms could also be varied: for example Bi has evaporation parameters [21] very similar to those of Pb and there should be no problems in the fabrication of a Sn–Bi alloy. Secondly a different substrate could be used, such as Ge(111), whose different lattice parameter and stiffness have been already demonstrated to critically influence the ground state properties of these metal induced reconstructions [22]. Ultimately, the controlled fabrication of such alloys could lead to a fine control of their Fermi surfaces and eventually drive the system into low temperature critical phenomena, such as those that have stimulated our study [1].

## Acknowledgments

CDT acknowledges financial support from the SOCRATES Project of the European Union. Valuable experimental support from Dr Jiri Slezák is also acknowledged. Financial support of the Czech Grant Agency is acknowledged: grant No 202/98/K002.

## References

[1] Carpinelli J M, Weitering H H, Plummer E W and Stumpf R 1996 *Nature* **381** 398
[2] Gauthier Y, Baudoing-Savois R, Bugnard J M, Hebenstreit W, Schmid M and Varga P 2000 *Surf. Sci.* **466** 155
[3] Ottaviano L, Ressel B, Di Teodoro C, Profeta G, Santucci S, Cháb V and Prince K C 2003 *Phys. Rev.* B **67** 045401
[4] Ressel B, Slezák J, Prince K C and Cháb V 2002 *Phys. Rev.* B **66** 035325
[5] Carpinelli J M, Weitering H H and Plummer E W 1998 *Surf. Sci.* **401** L457
[6] Yuhara J, Takada T, Nakamura D, Soda K and Kamada M 2002 *Mater. Sci. Eng.* B **96** 145
[7] Juré L, Magaud L, Mallet P and Veuillen J-Y 2000 *Appl. Surf. Sci.* **162** 638
[8] Kahng S-J, Park J-Y and Kuk Y 1999 *Surf. Sci.* **442** 379
[9] Olesinki R W and Abbaschian G J 1984 *Bull. Alloy. Phase Diagr.* **5** 271
[10] Okamoto H (ed) 2000 *Desk Handbook: Phase Diagrams for Binary Alloys* (Materials Park, OH: ASM International)
[11] Slezák J, Mutombo P and Cháb V 1999 *Phys. Rev.* B **60** 13328
[12] Ottaviano L, Profeta G, Continenza A, Santucci S, Freeman A J and Modesti S 2000 *Surf. Sci.* **464** 57
[13] Charrier A, Pérez R, Thibaudau F, Debever J-M, Ortega J, Flores F and Themlin J-M 2001 *Phys. Rev.* B **64** 115407
[14] Profeta G, Ottaviano L, Santucci S and Continenza A 2002 *Phys. Rev.* B **66** 081303
[15] Profeta G, Ottaviano L, Santucci S and Continenza A 2004 *Proc. Ecoss22 Conf.*; *Surf. Sci.* at press
[16] Moulder J F, Stickle W F, Sobol P E and Bomben K D 1992 *Handbook of X-ray Photoelectron Spectroscopy* ed J Chastain (Eden Prairie, MN: Perkin-Elmer)
[17] Feenstra R M, Stroscio J A and Fein A P 1987 *Surf. Sci.* **181** 295
[18] Ressel B, unpublished
[19] Kinoshita T, Kono S and Sagawa T 1986 *Phys. Rev.* B **34** 3011
[20] Carlisle J A, Miller T and Chiang T-C 1992 *Phys. Rev.* B **45** 3400
[21] Kim Y K, Kim J S, Hwang C C, Shrestha S P and Park C Y 2002 *Surf. Sci.* **498** 116
[22] Ballabio G, Profeta G, De Gironcoli S, Scandolo S, Santoro G E and Tosatti E 2002 *Phys. Rev. Lett.* **89** 126803